IMM vehicle tracking for traffic jam situations on highways

Nico Kaempchen, Klaus C.J. Dietmayer
University of Ulm
Dept. of Measurement, Control and Microtechnology
Albert–Einstein–Allee 41
D–89081 Ulm
Germany
nico.kaempchen@e-technik.uni-ulm.de

Abstract – *Classical vehicle tracking approaches for highway scenarios use a Kalman–filter with a single dynamic model optimised to a single driving manoeuvre. In contrast, the Interacting Multiple Model (IMM) filter allows for several parallel models which are combined to a weighted estimate. Choosing models for different driving modes such as constant speed, acceleration and strong acceleration changes permits the object state estimation to be optimised for highly dynamic driving manoeuvres. The paper describes the analysis of Stop&Go situations and the systematic parametrisation of the IMM method based on these statistics. The evaluation of the IMM approach is presented based on real sensor measurements of two laserscanners, a radar and a video image processing unit. The performance of the lateral estimation of the IMM is shown based on simulations.*

Keywords: Driver assistance systems, IMM, model–set design, traffic jam situations.

1 Introduction

Future driver assistance systems have increasing demand for a consistent and precise dynamic representation of the environment. The model based estimation of the dynamic parameters which describe the objects position, velocity and acceleration is of particular interest. Numerous publications describe object tracking approaches using a Kalman filter with linear dynamic models [1, 2, 3, 4]. Some approaches use non–linear models and are therefore based on an Extended Kalman filter [5]. All of these approaches, however, try to represent the dynamic behaviour of traffic participants by the use of a single general dynamic model. As the dynamic state of vehicles is highly variable over time, the general dynamic model has to meet the conditions of the most extreme situations as otherwise the filter is bound to be inconsistent in scenarios with high dynamic changes.

Recent research in the area of driver assistance systems takes multiple model approaches into account. Each model is designed to represent a certain mode or dynamic driving behaviour of an object. The aim is a situation adaptive estimation. In [6] the different models are switched depending on the actual dynamic situation. Problems are described concerning the tradeoff between switching delays and too frequent switches. Other approaches use the IMM filtering which enables a ”soft decision”. The final estimate is a weighted sum of several filter estimates which are based on different dynamic models [7, 8, 9].

This paper first describes the IMM algorithm. In section 3 the dynamic models and their parametrisation as well as the parametrisation of the IMM method based on the analysis of Stop&Go scenarios are systematically derived. The performance of the IMM approach is presented in section 4 with respect to a single Kalman filter implementation. Section 5 introduces a second IMM model–set design and presents its performance based on simulations and section 6 concludes the paper.

2 Interacting Multiple Model

The IMM method is composed of four main parts

- Interaction — the individual filter estimates are mixed with respect to the predicted model probabilities.
- Model specific filtering — each filter predicts and updates its state estimate using its dynamic model assumptions.
- Model probability update — the model probability of each model is updated with respect to the innovation error.
- Combination — for output purposes a combined state estimate is calculated from the weighted state estimates.

Following [10, 11, 12] the IMM algorithm is summarised below.

2.1 Interaction

The predicted model probability is given with the model probability of the previous cycle $\mu^{(j)}_{k-1|k-1}$ and π_{ji} which is the probability that the transition from state j to state i occurs

$$\mu^{(i)}_{k|k-1} = \sum_j \pi_{ji} \mu^{(j)}_{k-1|k-1} \tag{1}$$

With the conditional model probability, given the object is in state i that the transition occurred from state j

$$\mu^{(j|i)}_{k-1|k-1} = \frac{\pi_{ji} \mu^{(j)}_{k-1|k-1}}{\mu^{(i)}_{k|k-1}} \tag{2}$$

the mixing of the state estimates $\hat{\mathbf{x}}^{(j)}_{k-1|k-1}$ with their covariances $\mathbf{P}^{(j)}_{k-1|k-1}$ can be performed

$$\bar{\mathbf{x}}^{(i)}_{k-1|k-1} = \sum_j \mu^{(j|i)}_{k-1|k-1} \hat{\mathbf{x}}^{(j)}_{k-1|k-1} \quad (3)$$

$$\bar{\mathbf{P}}^{(i)}_{k-1|k-1} = \sum_j \mu^{(j|i)}_{k-1|k-1} [\mathbf{P}^{(j)}_{k-1|k-1} + (\bar{\mathbf{x}}^{(i)}_{k-1|k-1} - \hat{\mathbf{x}}^{(j)}_{k-1|k-1})(\bar{\mathbf{x}}^{(i)}_{k-1|k-1} - \hat{\mathbf{x}}^{(j)}_{k-1|k-1})'] \quad (4)$$

The probabilities π_{ji} that the transition from state j to state i occurs, are a design parameter of the IMM method. They are motivated by a Markovian switching process and will be discussed in section 3.3.

2.2 Model specific filtering

The predicted state estimates $\hat{\mathbf{x}}^{(i)}_{k|k-1}$ and their covariances $\mathbf{P}^{(i)}_{k|k-1}$ are calculated in our approach using an Extended Kalman filter. The different model assumptions will be discussed in section 3.1. The innovation is performed by calculation of the measurement residual $\mathbf{s}^{(i)}_k$, the residual covariance $\mathbf{S}^{(i)}_k$, the updated state estimate $\hat{\mathbf{x}}^{(i)}_{k|k}$ and its covariance $\mathbf{P}^{(i)}_{k|k}$.

2.3 Model probability update

The likelihood for the observation is calculated from the residual $\mathbf{s}^{(i)}_k$ assuming Gaussian statistics

$$L^{(i)}_k = \frac{\exp\left[-(1/2)(\mathbf{s}^{(i)}_k)'(\mathbf{S}^{(i)}_k)^{-1}\mathbf{s}^{(i)}_k\right]}{|2\pi\mathbf{S}^{(i)}_k|^{1/2}} \quad (5)$$

Thus, the predicted model probabilities $\mu^{(i)}_{k|k-1}$ are updated

$$\mu^{(i)}_{k|k} = \frac{\mu^{(i)}_{k|k-1} L^{(i)}_k}{\sum_j \mu^{(j)}_{k|k-1} L^{(j)}_k} \quad (6)$$

2.4 Combination

The overall state estimate $\hat{\mathbf{x}}_{k|k}$ and its covariance $\mathbf{P}_{k|k}$ are a weighted combination of the model state estimates $\hat{\mathbf{x}}^{(i)}_{k|k}$ and their covariances $\mathbf{P}^{(i)}_{k|k}$

$$\hat{\mathbf{x}}_{k|k} = \sum_i \mu^{(i)}_k \hat{\mathbf{x}}^{(i)}_{k|k} \quad (7)$$

$$\mathbf{P}_{k|k} = \sum_i \mu^{(i)}_{k|k} [\mathbf{P}^{(i)}_{k|k} + (\hat{\mathbf{x}}_{k|k} - \hat{\mathbf{x}}^{(i)}_{k|k})(\hat{\mathbf{x}}_{k|k} - \hat{\mathbf{x}}^{(i)}_{k|k})'] \quad (8)$$

3 Model–set design

In order to focus on the examination of the IMM filter performance, we concentrated on Stop&Go driving situations. Extended data from the Inertial Navigation System (INS) of motorway traffic jams was analysed concerning the velocity, acceleration and yaw rate in order to determine the different driving modi. From those, the models of the IMM model–set were derived.

Figure 1 shows the velocity in a Stop&Go situation. The sequence is divided into sections of almost constant

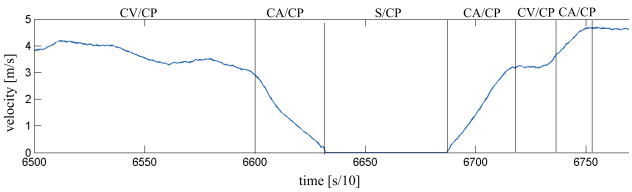

Fig. 1: Analysis of a Stop&Go situation.

dynamic behaviour. For the longitudinal dynamics four classes are considered: stationary (S), constant velocity (CV), constant acceleration (CA) and a class representing a maneuver change. The lateral dynamics are separated into constant yaw angle ψ (CP) and varying yaw angle.

In order to prevent a too frequent switching between the states, slight deviations from the dynamic constraints are allowed. The degree of deviation is determined by the choice of the model noise.

3.1 Dynamic Models

The dynamic modelling of the Extended Kalman–filter kernels used in the IMM method determines the constraints of the dynamic process. Two different general model groups are considered. The free motion model and the bicycle model. In the case of the latter model the motion is directed into the objects orientation neglecting the slip of the wheels.

3.1.1 Free motion model

The dynamic state of the constant acceleration model is given by $\mathbf{x}_{CA} = [x, y, \psi, v_x, v_y, a_x, a_y]'$ where $[x, y]'$ is the position, ψ the yaw angle, $[v_x, v_y]'$ the velocity vector and $[a_x, a_y]'$ the acceleration vector.

For the model of constant acceleration the dynamics are given by

$$\dot{\mathbf{x}}_{CA} = \begin{bmatrix} v_x \\ v_y \\ 0 \\ a_x \\ a_y \\ 0 \\ 0 \end{bmatrix} + \begin{bmatrix} 0 \\ 0 \\ n_\psi \\ 0 \\ 0 \\ n_{a_x} \\ n_{a_y} \end{bmatrix} \quad (9)$$

where n_ψ, n_{a_x} and n_{a_y} are white noise terms which account for the errors made by the model assumption of constant acceleration and constant yaw angle.

The state vector of the constant velocity model is $\mathbf{x}_{CV} = [x, y, \psi, v_x, v_y, a_x = 0, a_y = 0]'$. The differential equation describing the constant velocity model is given by

$$\dot{\mathbf{x}}_{CV} = \begin{bmatrix} v_x \\ v_y \\ 0 \\ 0 \\ 0 \\ 0 \\ 0 \end{bmatrix} + \begin{bmatrix} 0 \\ 0 \\ n_\psi \\ n_{v_x} \\ n_{v_y} \\ 0 \\ 0 \end{bmatrix} \quad (10)$$

where n_{v_x} and n_{v_y} are white noise terms which account for the errors made by the constant velocity assumption.

The state vector of the stationary model is $\mathbf{x}_S = [x, y, \psi, v_x = 0, v_y = 0, a_x = 0, a_y = 0]'$. The differential equation describing the stationary model is given by

$$\dot{\mathbf{x}}_S = \begin{bmatrix} n_x & n_y & n_\psi & 0 & 0 & 0 & 0 \end{bmatrix}' \tag{11}$$

where n_x and n_y are white noise terms which account for the errors made by the model assumption.

3.1.2 Simplified bicycle model

The dynamic state of the model is given by $\mathbf{x} = [x, y, \psi, v, \omega, a]'$ where $[x, y]$ is the position, ψ the yaw angle, v the velocity, ω the yaw rate and a the acceleration. The orientation of the velocity and acceleration vectors are here defined by the yaw angle as shown in figure 2.

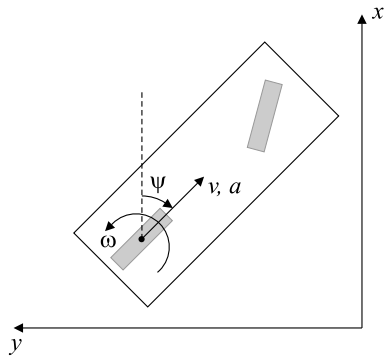

Fig. 2: Simplified bicycle model of the kinematic behaviour of a vehicle. The orientation of the velocity and acceleration vectors are defined by the yaw angle ψ and yaw rate ω.

The differential equation describing a constant acceleration and constant yaw rate is approximated by

$$\dot{\mathbf{x}}_{VCA} = \begin{bmatrix} v\cos(\psi) \\ v\sin(\psi) \\ \omega \\ a \\ 0 \\ 0 \end{bmatrix} + \begin{bmatrix} 0 \\ 0 \\ 0 \\ 0 \\ n_\omega \\ n_a \end{bmatrix} \tag{12}$$

Note that the influence of the yaw rate ω on the position is neglected. n_a and n_ω are white noise terms which account for the errors made by the constant acceleration and constant yaw rate assumption.

The differential equation describing a constant velocity and constant yaw angle is

$$\dot{\mathbf{x}}_{VCV} = \begin{bmatrix} v\cos(\psi) \\ v\sin(\psi) \\ 0 \\ 0 \\ 0 \\ 0 \end{bmatrix} + \begin{bmatrix} 0 \\ 0 \\ n_\psi \\ n_v \\ 0 \\ 0 \end{bmatrix} \tag{13}$$

where n_v and n_ψ are white noise terms which account for the errors made by the constant velocity and constant yaw angle assumption.

The equation describing the stationary model is equal to the free motion stationary model

$$\dot{\mathbf{x}}_{VS} = \dot{\mathbf{x}}_S \tag{14}$$

3.2 Model noise covariance

The model noise covariance matrix $\mathbf{Q}_k$ at time k is calculated using the direct discrete white noise approach, where Γ is the noise gain and σ^2 the variance of the process noise [10]

$$\mathbf{Q}_k = \Gamma_k \sigma^2 \Gamma_k' \tag{15}$$

A first estimation of the standard deviation of the model noise σ is given by the allowed deviation in the labelling process described above. In order to find the optimal noise level, sequences of measurements are chosen which meet the different model assumptions. Using hypothesis testing techniques the process noise can be optimised with respect to peak–RMS errors and mean–RMS errors.

3.3 Markov transition probability matrix

The diagonal elements of the transition matrix represent the probability that the object remains in mode i. Following [11] they are related to the mean sojourn times (τ_i) and the sampling interval T

$$\pi_{ii} = 1 - \frac{T}{\tau_i} \tag{16}$$

The mean sojourn time as well as the off–diagonal elements are derived from the statistics of the above mentioned analysis of the Stop&Go scenario. If n_{ij} is the counted number of transitions from mode i to mode j and n_i is the sum of all transitions from mode i, the transition probabilities are given by

$$\pi_{ij} = \frac{n_{ij}}{n_i}(1 - \pi_{ii}) \tag{17}$$

4 Results based on Real Measurements

4.1 Experimental setup and system architecture

The experimental setup for evaluation of different IMM implementations is composed of two test vehicles. The ego–vehicle is equipped with an Inertial Navigation System (INS), a GPS sensor and several forward looking sensors.

Two infrared Laserscanners are mounted at the left and right side of the front bumper, thus covering the region left, right and in front of the ego–vehicle. The object recognition range is up to 60 m. The pre–processed measurements which are delivered to the fusion system are a three point contour description of the detected objects.

A 77 GHz long range radar measures the relative position and radial velocity of objects. The field of view is limited to 6° azimuth angle and 120 m distance.

Additionally a monocular vision system, mounted behind the frontal windscreen, detects vehicles and estimates the lane position and curvature. The horizontal aperture is 22° and the detection range up to 70 m.

The target–vehicle is equipped with an INS which measures the vehicles dynamic state and with a GPS sensor in order to synchronise the sensor measurements with the ego–vehicle.

The IMM algorithm is integrated into a centralised event–triggered sensor fusion architecture described in [13]. The measurements are chronologically ordered, thus introducing an additional delay, which can in turn be minimized if the sensor measurement times are predictable [14]. The performance is evaluated using predefined driving maneuvers.

4.2 Model–set parameters

For highway scenarios the free motion models described in section 3.1.1 performed better than the bicycle models described in section 3.1.2. For traffic jam situations a model–set composed of three models was found to be suitable.

The first model is a stationary model where the standard deviation of the noise in the position estimate is

$$\sigma_x = \sigma_y = 0.32 \, \frac{m}{s} \tag{18}$$

The noise in the yaw angle is given by

$$\sigma_\psi = 0.04 \, \frac{rad}{s} \tag{19}$$

The constant velocity model is parametrised with

$$\sigma_{vx} = \sigma_{vy} = 0.89 \, \tfrac{m}{s^2} \tag{20}$$

$$\sigma_\psi = 0.12 \, \tfrac{rad}{s} \tag{21}$$

The model of constant acceleration has a high model noise with standard deviations of

$$\sigma_{ax} = 8.0 \, \tfrac{m}{s^3} \tag{22}$$

$$\sigma_{ay} = 2.0 \, \tfrac{m}{s^3} \tag{23}$$

$$\sigma_\psi = 0.25 \, \tfrac{rad}{s} \tag{24}$$

This model is designed to fit phases of constant acceleration and acceleration changes, as well as lane changes.

The Markov matrix $\mathbf{P}(T)$ is determined from the statistics of traffic jam situations:

$$\mathbf{P}(0.1\ sec) = \begin{bmatrix} 0.980 & 0.000 & 0.020 \\ 0.000 & 0.970 & 0.030 \\ 0.003 & 0.017 & 0.980 \end{bmatrix} \tag{25}$$

The transition probabilities are adapted in each cycle with respect to the actual sampling interval. The initial model probabilities are chosen as

$$\mu = \begin{bmatrix} 0.333 & 0.333 & 0.334 \end{bmatrix}' \tag{26}$$

The IMM based on this model–set is compared to a single constant velocity Kalman–filter with

$$\sigma_{vx} = 2.0 \, \tfrac{m}{s^2} \tag{27}$$

$$\sigma_{vy} = 0.2 \, \tfrac{m}{s^2} \tag{28}$$

$$\sigma_\psi = 2.0 \, \tfrac{rad}{s} \tag{29}$$

4.3 Strong acceleration changes

In Stop&Go conditions, potentially very harmful situations occur at the end of traffic jams. Cars driving at high speed suddenly start breaking or even worse, have to brake from an acceleration phase.

In figure 3 such a driving maneuver is shown. The true velocity v_t recorded from the target–vehicle exhibits the strong acceleration and then strong deceleration behaviour. The error in the estimated velocity v_e of the target–vehicle observed from the ego–vehicle is shown below. As expected, the estimation error of a single constant velocity Kalman–filter is high at acceleration phases as the model assumption does not meet the dynamics of the situation. The IMM method switches from the stationary to the constant acceleration model within few sampling intervals. Once the acceleration is finished the model probability for the model of constant velocity increases. However, as soon as the deceleration process starts the constant acceleration model again gains the highest probability. Thus, the IMM approach reduces the estimation error significantly in acceleration phases compared to the single Kalman–filter implementation.

Figure 4 shows the estimated standard deviation of the velocity σ_v. The uncertainties in the estimation are almost constant for the Kalman–filter of constant velocity. The estimated standard deviation of the IMM method, however, exhibits a strong variation. In phases of no motion, the uncertainties are quite low and as soon as the acceleration begins the standard deviation increases. This situation adaptive uncertainty in the estimation process is an important feature of the IMM approach as in tracking systems the measurement association gate depends on the estimated standard deviation. If the uncertainty is estimated too low, the object might be lost. However, using an IMM approach, the estimated standard deviation can be adapted to the driving situation. In our case, the standard deviation raises in

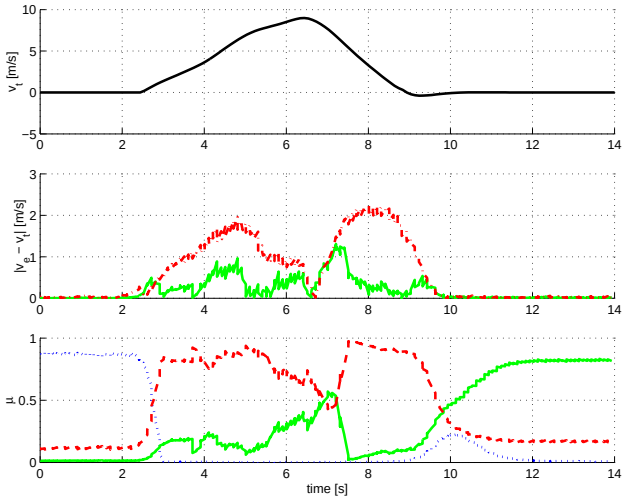

Fig. 3: Velocity v_t recorded in target–vehicle. Errors in estimated velocity v_e of single a Kalman–filter (CV) (dashed red) and of the IMM method (solid green). Model probabilities μ of IMM: Stationary (dotted blue), Constant velocity (solid green), constant acceleration (dashed red).

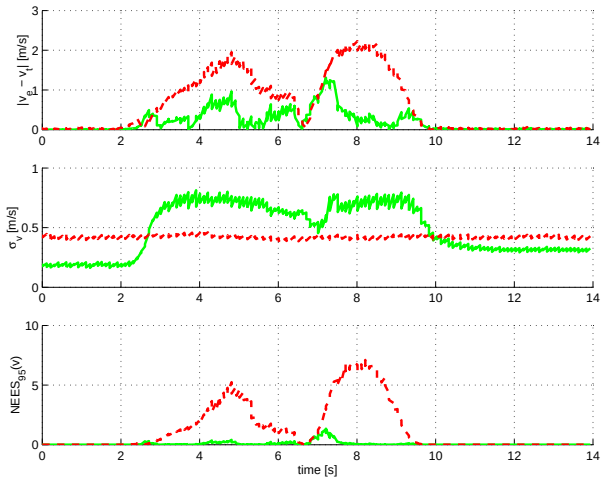

Fig. 4: Errors in estimated velocity v_e of single Kalman–filter (CV) (dashed red) and of IMM (solid green). Estimated standard deviation of velocity σ_v. NEES of velocity normalized to its 95% probability region.

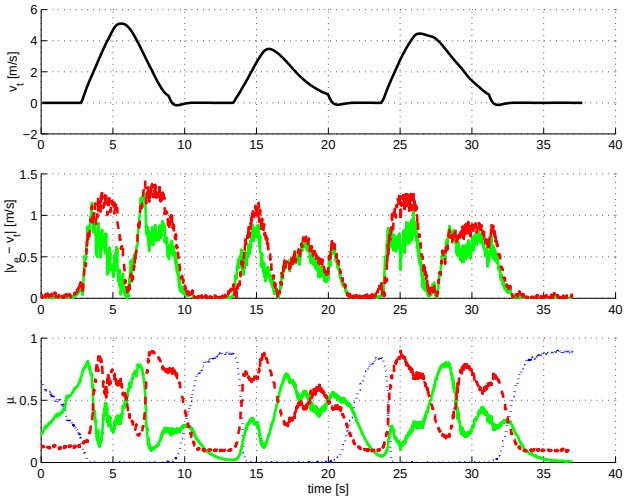

Fig. 5: Velocity v_t recorded in target–vehicle. Errors in estimated velocity v_e of single a Kalman–filter (CV) (dashed red) and of the IMM method (solid green). Model probabilities μ of IMM: Stationary (dotted blue), Constant velocity (solid green), constant acceleration (dashed red).

phases of high dynamics. Therefore the association gate is enlarged and the object is more likely to be continuously tracked.

The normalised estimation error squared (NEES) expresses the filter consistency [10]. Figure 4 shows the NEES of the velocity estimate normalized to a 95% probability region, assuming a χ^2 distribution. The normalized NEES of the single Kalman–filter is most of the time above 1.0, i.e. the estimated filter uncertainty is not consistent with the true estimation error considering the 95% probability region. Conversely, the estimation of the IMM method is consistent during the whole maneuver.

4.4 Stop&Go

Traffic jam situations are characterised by cars driving at low speed, accelerating, decelerating and stopping. These different driving maneuvers can change in rapid succession. In figure 5 such a driving maneuver is shown. The true velocity v_t recorded by the target–vehicle exhibits first a standstill and an acceleration directly followed by a deceleration to a halt. This pattern is repeated twice.

With its four sensors the ego–vehicle measures position and velocity of the target–vehicle. The error in the estimated velocity v_e is shown below. The error of the single constant velocity Kalman–filter is high during acceleration and deceleration phases. The IMM implementation can however reduce the error in the acceleration phase after a short period of adaption. The model probabilities $\mu^{(i)}$ show that the IMM method switches at the beginning of acceleration phases from the stationary model to the constant acceleration model. As the acceleration is only about 2 $\frac{m}{s^2}$, the probability of the constant velocity model rises again. This has the effect that the error reduction of the IMM method compared to the single Kalman–filter is significant, but not as high as expected. Using four models, with an additional model for constant acceleration with very low process noise did not improve the results, as the switching across the different models takes too long when compared to the duration of the maneuver.

Figure 6 shows the estimated standard deviation of the velocity σ_v. The uncertainties in estimation are almost constant for the Kalman–filter of constant velocity. The estimated standard deviation of the IMM method however exhibits a strong variation. In phases of standstill, the IMM–estimated standard deviation is significantly lower compared to that of the Kalman–filter alone. This enables a noise reduction of more than 50% compared to the single Kalman–filter. As soon as the acceleration or deceleration begins the standard deviation of the IMM method increases again.

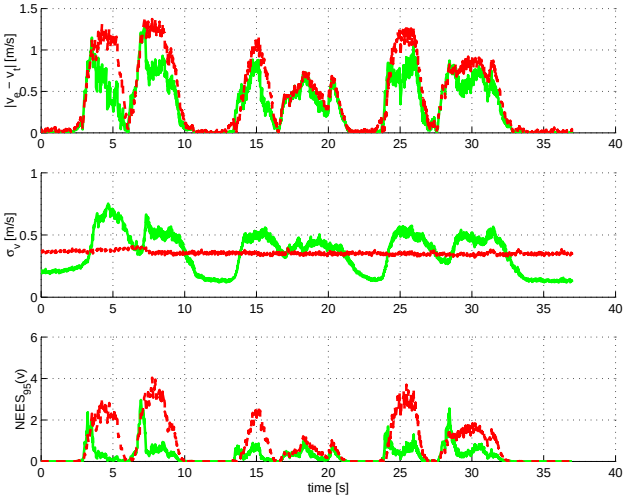

Fig. 6: Errors in estimated velocity v_e of single Kalman–filter (CV) (dashed red) and of IMM (solid green). Estimated standard deviation of velocity σ_v. NEES of velocity normalized to its 95% probability region.

The normalized NEES of the single Kalman–filter is in phases of acceleration most of the time above 1.0, i.e. the

estimated filter uncertainty is not consistent with the true estimation error considering the 95% probability region. In contrast the IMM–estimation is consistent during almost the whole maneuver. Exceptions are at the beginning of the acceleration when the model probability of the acceleration model is still increasing. This is due to the maneuver detection delay of the IMM approach.

5 Results based on simulations

The above shown performance of the IMM using three models with stationary, constant velocity and constant acceleration Kalman–filter kernels proved to be superior to a single constant velocity Kalman–filter. There are however some disadvantages in the choice of this model–set.

Using filter kernels of different polynomial orders (e.g. a model–set containing constant acceleration and constant velocity models) results in an underestimation of higher order parameters (the acceleration) of the combined state vector in phases where the dynamic situation is not exactly represented by a model. This is almost always true in traffic situations and in particular in traffic jams. We suggest therefore that the model–set should contain only models of the same order, if higher order parameters are of interest for instance for a controller. As an example, consider an IMM with a constant velocity and a constant acceleration filter kernel. If the observed object drives at constant speed with short weak acceleration intervals, the model probability of the constant acceleration model is never very high. Therefore, the mixed estimate of the acceleration parameter is always an underestimation of the true acceleration, even if the constant acceleration model has low estimation errors.

Additionally, the above presented examples only show the performance in the longitudinal direction. The performance of the lateral estimation could not be determined based on real measurements, due to the lack of a full reference trajectory. In simulations it can be shown that the lateral estimate of the investigated model–set performs well in traffic–jams on highways. However, in urban areas, cars may turn abruptly at crossings. This dynamic situation can be better represented by coordinated turn models or the above mentioned bicycle models.

Based on these criterions a new model–set is designed, based on the bicycle model.

5.1 Model–set parameters

Two white noise constant acceleration bicycle models are chosen.

The first model of constant acceleration has a low model noise with standard deviations of

$$\sigma_a = 0.4 \ \frac{m}{s^3} \tag{30}$$

$$\sigma_\omega = 0.1 \ \frac{rad}{s^2} \tag{31}$$

This model is designed to fit phases of constant acceleration and constant turning.

The second model of constant acceleration has a high model noise with standard deviations of

$$\sigma_a = 12.0 \ \frac{m}{s^3} \tag{32}$$

$$\sigma_\omega = 2.6 \ \frac{rad}{s^2} \tag{33}$$

This model is designed to fit phases of acceleration changes, lane changes and transitions from straight driving to turning at a crossing.

The Markov matrix $\mathbf{P}(T)$ is determined from the statistics of traffic jam situations:

$$\mathbf{P}(0.1 \ sec) = \begin{bmatrix} 0.97 & 0.03 \\ 0.05 & 0.95 \end{bmatrix} \tag{34}$$

The transition probabilities are adapted in each cycle with respect to the actual sampling interval. The initial model probabilities are chosen as $\mu = \begin{bmatrix} 0.5 & 0.5 \end{bmatrix}'$.

5.2 Simulation setup

The trajectories of the simulation data are derived from the data acquired by the INS of a test vehicle. The resulting trajectories are the natural paths of vehicles driving in typical scenarios. The measurement vector is composed of the position $[x, y]'$ and the yaw angle ψ. Gaussian noise was added to the data with $\sigma_x = \sigma_y = 0.1$ m and $\sigma_\psi = 0.5$ rad, thus simulating the measurements of a single Laserscanner at 10 Hz scan frequency. The measurement interval is 100 ms.

5.3 Turning

Figure 7 shows the estimated yaw angle ψ of a turning car.

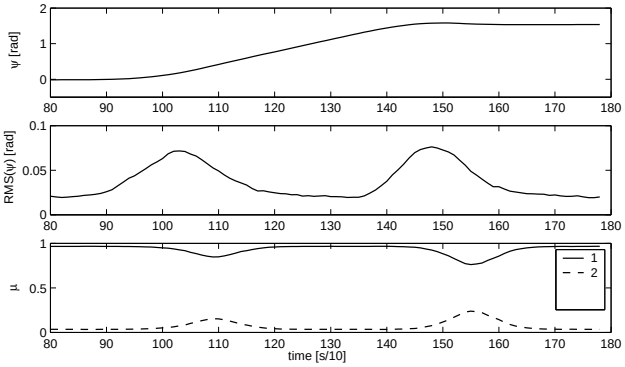

Fig. 7: Yaw angle ψ, RMS(ψ) and model probabilities.

The yaw angle is well estimated and the mean–RMS of 500 Monte–Carlo runs in the non–maneuver phase is of the order of $\frac{1}{25}$ of the measurement noise. This high noise reduction of the yaw measurements can be explained by the kinematic restrictions of the dynamic model and the relatively low noise in the position measurements. Even the peak–RMS of 0.067 rad is low. The model probabilities show that the probability of the second model raises in phases of transition between straight driving and turning. However the increase in the model probability is not very high, as the transition is itself blurred over time. The first model is therefore able to cope with this weak violation of the model assumptions. In the following paragraphs it will be shown that the increase in probability of the second model is proportional to the extent of the violation of the dynamic model assumptions. Figure 8 shows the estimated yaw rate of the turning car.

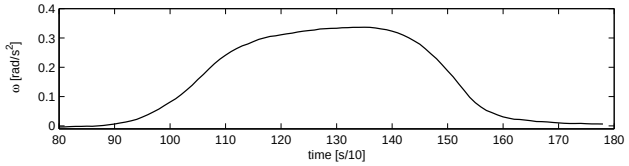

Fig. 8: Estimated yaw rate ω.

5.4 Strong acceleration changes

Figure 9 shows the estimated velocity v and acceleration a of a vehicle which accelerates and then directly brakes. The gear change from first to second gear can be noted at measurement intervals 80–85. The model probabilities are

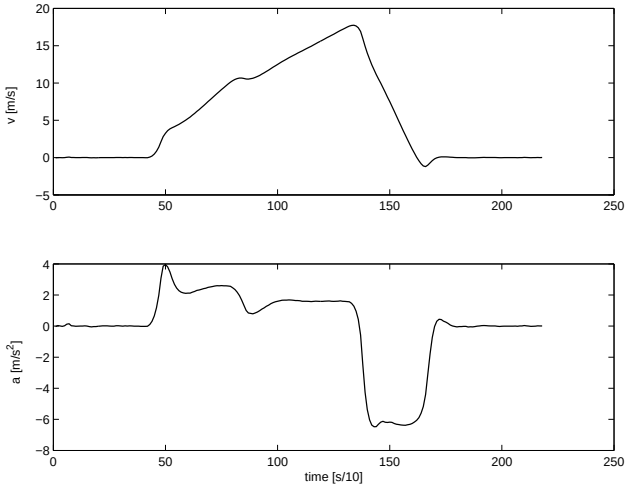

Fig. 9: Estimated velocity v and the estimated acceleration a.

shown in figure 10. Again the probability of the second model rises at strong acceleration changes. Here the increase is highly significant, especially at the transition from the acceleration to the deceleration phase when the change in acceleration is of a magnitude of 12 m/s^3.

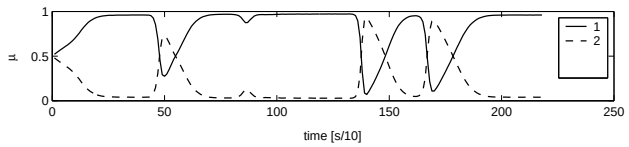

Fig. 10: Model probabilities.

The standard deviation of 500 Monte–Carlo runs in figure 11 exhibits a good noise reduction. However, the mean estimation error $e_v(k) = E\{v(k) - \hat{v}(k)\}$ of the velocity estimate has a maximum of 1.05 m/s. The mean estimation error is a quantitative criterion for the performance of the filter in highly dynamic scenarios.

The standard deviation $\sigma_v(k) = E\{[\hat{v}(k) - E\{\hat{v}\}]^2\}^{\frac{1}{2}}$ of the estimation error is a quantitative criterion for the noise reduction ability of the filter. In non–maneuver phases the standard deviation is in the magnitude of 0.2 m/s. In times of a transition between different accelerations the standard deviation increases up to 0.4 m/s within 3–4 measurement intervals. This increase is due to the high probability of the

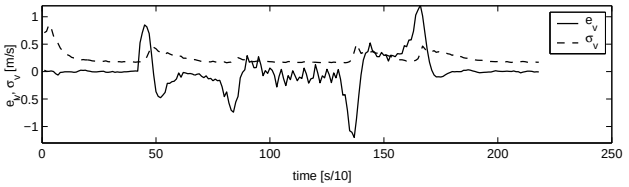

Fig. 11: Mean estimation error and its standard deviation of the velocity estimate v.

Kalman–filter kernel with the high model noise. The general noise reduction is therefore satisfactory. Only at transition times when the assumptions of the dynamic model are violated, does the noise reduction decrease.

5.5 Extreme turning scenarios

Figure 12 shows the estimated yaw angle ψ of a car performing extreme right followed fast by extreme left turns. The yaw angle is well estimated and the mean–RMS of 500

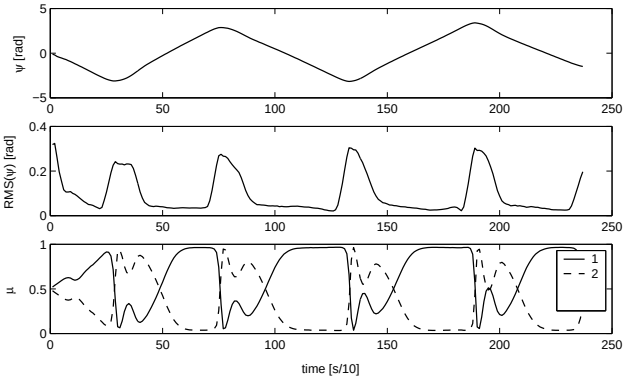

Fig. 12: Yaw angle ψ, RMS(ψ) and model probabilities.

Monte–Carlo runs is of the order of $\frac{1}{10}$ of the measurement noise. The peak–RMS of 0.3 rad is high, though still below the measurement noise. The model probabilities show that the second model takes over in phases of transition between the left and right turning. Figure 13 shows the estimated yaw rate.

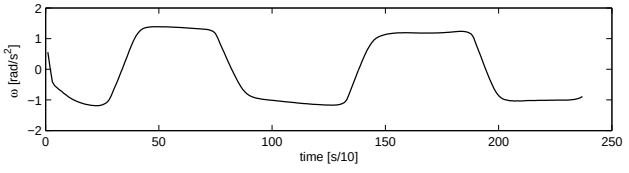

Fig. 13: Estimated yaw rate ω.

5.6 Conclusion for simulations

These simulations show that the chosen two model IMM with underlying bicycle models performs well in longitudinally and laterally challenging driving scenarios. The first Kalman–filter is designed for scenarios of almost constant acceleration and turning. Small deviations of the assumption are accounted for by a low model noise. The second Kalman–filter kernel is increased in its weight in situations

where the almost constant acceleration and yaw rate assumption is violated. The weight depends on the extent of the violation. The stronger the acceleration or yaw rate changes, the higher is the estimated probability of the second model with high model noise. This two Kalman–filter based IMM implementation therefore exhibits a good noise reduction in normal driving situations and at the same time a high flexibility in highly dynamic lateral and longitudinal scenarios.

6 Conclusion

A systematic parametrisation of the IMM approach based on the analysis of Stop&Go situations is presented. In situations of high dynamics, the IMM method is able to reduce the estimation errors significantly compared to single Kalman–filter approaches, due to its situation adaptive dynamic estimation. The performance was evaluated and optimised in simulations and presented with real measurements of two laserscanners, a radar and an image processing unit. Future work could use the probabilities of the different dynamic models for a situation analysis. This can for instance enable the detection of traffic jams or lane changes.

Acknowledgements

The work was supported by the VOLKSWAGEN AG, Wolfsburg, Germany.

References

[1] C. Stiller, J. Hipp, C. Rössig, and A. Ewald. Multisensor obstacle detection and tracking. *Image and Vision Computing*, 18:389–396, 2000.

[2] Jan C. Becker. Fusion of Data from the Object-Detection Sensors of an Autonomous Vehicle. In *IEEE Conference on Intelligent Transportation Systems 1999*, Tokyo, Japan, 1999.

[3] Kay Ch. Fuerstenberg, Klaus C. J. Dietmayer, Stephan Eisenlauer, and Volker Willhoeft. Multilayer laserscanner for robust object tracking and classification in urban traffic scenes. In *Proceedings of ITS 2002, 9th World Congress on Intelligent Transportation Systems*, Chicago, October 2002.

[4] H. Cramer, U. Scheunert, and G. Wanielik. Multi sensor fusion for object detection using generalized feature models. In *6th International Conference on Information Fusion*, pages 2–10, Cairns, Australia, July 2003.

[5] Frank Dellaert, Dean Pomerleau, and Chuck Thorpe. Model-Based Car Tracking Integrated with a Road-Follower. In *Proceedings of the 1998 IEEE International Conference on Robotics and Automation*, Leuven, Belgium, May 1998.

[6] Kristian Weiss, Dirk Stueker, and Alexander Kirchner. Target Modeling and Dynamic Classification for Adaptive Sensor Data Fusion. In *Proceedings on IEEE Intelligent Vehicles Symposium*, pages 132–137, June 2003.

[7] Liang Zhao and Chuck Thorpe. Qualitative and Quantitative Car Tracking from a Range Image Sequence. In *IEEE Computer Society Conference on Computer Vision and Pattern Recognition 1998*, pages 496–501, Santa Barbara, CA, June 1998.

[8] A. Amditis, A. Polychronopoulos, I. Karaseitanidis, G. Katsoulis, and E. Bekiaris. Multiple-sensor-collision avoidance system for automotive applications using an imm approach for obstacle detection. In *5th International Conference on Information Fusion*, pages 812–817. ISIF, 2002.

[9] Rainer Möbus, Armin Joos, and Uli Kolbe. Multi-target multi-object radartracking. In *Proceedings on IEEE Intelligent Vehicles Symposium*, pages 489–494, June 2003.

[10] Yaakov Bar-Shalom. *Estimation and Tracking: principles, techniques, and software*. Norwood, MA, artech house edition, 1993.

[11] Samuel S. Blackman and Robert Popoli. *Design and Analysis of Modern Tracking Systems*. Norwood, MA, artech house edition, 1999.

[12] Yaakov Bar-Shalom and William Dale Blair, editors. *Multitarget-Multisensor Tracking: Applications and Advances*, volume 3. Norwood, MA, artech house edition, 2000.

[13] A. Vukotich and Alexander Kirchner. Sensor fusion for driver-assistance-systems. In *Elektronik im Kraftfahrzeug*, Baden-Baden, Germany, 2001.

[14] Nico Kaempchen and Klaus C. J. Dietmayer. Data synchronization strategies for multi-sensor fusion. In *Proceedings of ITS 2003, 10th World Congress on Intelligent Transportation Systems*, Madrid, Spain, November 2003.